Control of a Forced Impacting Hertzian Contact Oscillator Near Sub- and Superharmonic Resonances of Order 2

Amine Bichri

Mohamed Belhaq

University Hassan II-Casablanca,
Laboratory of Mechanics,
Casablanca, Morocco

The effect of a fast harmonic base displacement and of a fast periodically time varying stiffness on vibroimpact dynamics of a forced single-sided Hertzian contact oscillator is investigated analytically and numerically near sub- and superharmonic resonances of order 2. The study is carried out using averaging procedure over the fast dynamic and applying a perturbation analysis on the slow dynamic. The results show that a fast harmonic base displacement shifts the location of jumps, triggering the vibroimpact response, toward lower frequencies, while a fast periodically time-varying stiffness shifts the jumps toward higher frequencies. This result has been confirmed numerically for both sub- and superharmonic resonances of order 2. It is also demonstrated that the shift toward higher frequencies produced by a fast harmonic parametric stiffness is larger than that induced by a fast base displacement. [DOI: 10.1115/1.4004309]

Keywords: Hertzian contact, vibroimpact, fast excitation, subharmonic resonance, superharmonic resonance, control

1 Introduction

Vibroimpact dynamic usually arises in engineering applications as in rolling contact mechanism, bearing, gear drive, and in mechanisms transforming rotation or translations. Such systems have been considered and investigated in a series of papers; see, for instance, Refs. [1–5], and references therein. In these later studies, a single-degree-of-freedom system was considered for modeling the behavior of a moving surface under a Hertzian contact force. The dynamic of an idealized preloaded and nonsliding dry Hertzian contact was studied near the primary resonance [6] and near the subharmonic [7] and the superharmonic [8] resonances of order 2. The analysis was based on numerical simulations, analytical approximation, and experimental testing. It was concluded that the vibroimpact responses resulting from the loss of contact are principally initiated by jumps near these resonances (the primary, sub- and superharmonic) and the nonlinearity in the Hertzian contact law has to be taken into consideration in order to predict the birth of these vibroimpact responses. Therefore, to have the system operating in a desired interval of the basic excitation frequency without the loss of contact, it is necessary to develop strategies for controlling the location of jumps near resonances. In this context, three strategies were proposed recently to control the location of jumps near the principal resonance of a Hertzian contact oscillator [9]. The first strategy introduces a fast harmonic force added to the basic harmonic forcing from above, the second one uses a fast harmonic base displacement, while the third strategy considers a rapidly and periodically time-varying stiffness. It was shown that a fast excitation from above or through a base displacement causes the resonance curve to shift left, whereas the rapidly parametric stiffness shifts the response curve right. It was also concluded that from a practical point of view, the first strategy (harmonic force from above) is not suitable because the amplitude level of excitation needed to realize a significant shift is too high. In contrast, the other two strategies (base displacement and parametric stiffness) can be used in practice to produce a shift with relatively small amplitude level of excitation.

To complete the previous study [9], the present work deals with the control of jumps near sub- and superharmonic resonances of order 2 in a forced Hertzian contact oscillator [9]. Attention is focused on the two suitable control strategies, namely the fast base displacement and the fast time-varying stiffness.

It is worth noticing that the fast excitations has been widely used over the past decades for control purpose; see the pioneer works [10–12]. For applications including control of stability, stiffness, frequencies, resonance, limit cycle, delay, hysteresis and pull-in in MEMS, see Refs. [13–22].

The rest of the paper is organized as follows. The next section deals with the control of a forced Hertzian contact oscillator using a fast harmonic base motion. The analysis is carried out in the vicinity of the sub- and superharmonic resonance of order 2. An averaging technique is performed to obtain the slow dynamic and the multiple scale method is applied on the slow dynamic to derive the corresponding modulation equations. Analysis of equilibria of the slow flow is performed and the frequency responses are examined. Section 3 follows a similar analysis, as in Sec. 2, in the case where a fast time-varying stiffness is applied. Section 4 compares the effect of the fast harmonic base displacement and the effect of the fast parametric stiffness on the frequency response near the sub- and superharmonic resonances of order 2. Section 5 concludes the work.

2 Case of a Fast Harmonic Base Motion

In this section, we investigate the effect a fast harmonic base motion on the frequency response of a forced single-sided Hertzian contact system near the sub- and superharmonic resonances of order 2. The schematic model with a harmonic base motion is shown in Fig. 1 and the equation of motion is written as [9]

$$m\ddot{z} + c(\dot{z} - \dot{z}_e) + k(z - z_e)^{3/2} = N(1 + \sigma\cos\omega t) \qquad (1)$$

where z is the normal displacement of the rigid mass m, c the damping coefficient, k the constant given by the Hertzian theory, N the static normal force, σ and ω are the level of the excitation

Contributed by the Design Engineering Division of ASME for publication in the Journal of Computational and Nonlinear Dynamics. Manuscript received March 13, 2011; final manuscript received May 23, 2011; published online July 22, 2011. Assoc. Editor: José L. Escalona.

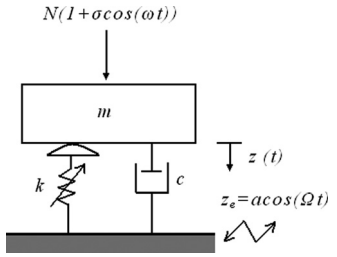

Fig. 1 Schematic model in the case of a rapid harmonic base motion

and its frequency, respectively. Here $z_e = a\cos\Omega t$ is the fast harmonic base motion with a and Ω are the amplitude and the frequency of the excitation, respectively. Equation (1) can be written in the dimensionless form as

$$\ddot{q} + 2\xi(\dot{q} - \dot{q}_e) + \left(1 + \frac{2}{3}(q - q_e)\right)^{3/2} = 1 + \sigma\cos\bar{\omega}\tau \tag{2}$$

where $\bar{\omega} = (\omega/\nu)$, $\nu^2 = (3k/2m)z_s^{1/2}$, $\xi = c/2m\nu$, $q = 3(z - z_s)/2z_s$, $\tau = \nu t$, $\bar{\Omega} = (\Omega/\nu)$, $z_s = (N/k)^{2/3}$, and $q_e = \frac{3}{2}(z_e/z_s)$.

Using a truncated Taylor series of the term $(1 + \frac{2}{3}(q - q_e))^{3/2}$ around the origin and q_e and substituting into Eq. (2), one obtains the following equation:

$$\ddot{q} + q + \alpha\dot{q} + \beta q^2 - \gamma q^3 = \sigma\cos\bar{\omega}\tau + \alpha\dot{q}_e + \left(1 + 2\beta q - \frac{\beta}{3}q^2 + \gamma q^3\right)q_e \tag{3}$$

where $\alpha = 2\xi$, $\beta = \frac{1}{6}$, $\gamma = \frac{1}{54}$, $q_e = \bar{a}\cos\bar{\Omega}\tau$, and $\bar{a} = \frac{3a}{2z_s}$. The slow dynamic corresponding to Eq. (3) is obtained using the method of direct partition of motion [24,25]. Introducing two different time scales, a fast time $T_0 = \bar{\Omega}\tau$ and a slow time $T_1 = \tau$, splitting up $q(\tau)$ into a slow part $x(T_1)$ and a fast part $\varepsilon\psi(T_0, T_1)$ as

$$q(\tau) = x(T_1) + \psi(T_0, T_1) \tag{4}$$

where x describes the slow main motions at time scale of oscillations, ψ stands for an overlay of the fast motions. The frequency Ω is considered as a large parameter, for convenience. The fast part $\varepsilon\psi$ and its derivatives are assumed to be $2\pi-$periodic functions of fast time T_0 with zero mean value with respect to this time, so that $\langle q(t)\rangle = x(T_1)$ where $\langle\cdots\rangle \equiv (1/2\pi)\int_0^{2\pi}(\cdots)dT_0$ defines time-averaging operator over one period of the fast excitation with the slow time T_1 fixed.

Introducing $D_i^j \equiv \partial^j/\partial^j T_i$ yields $d/dt = \Omega D_0 + D_1$, $d^2/dt^2 = \Omega^2 D_0^2 + 2\Omega D_0 D_1 + D_1^2$, and substituting Eq. (4) into Eq. (3) gives

$$\ddot{x} + \ddot{\psi} + x + \psi + \alpha\dot{x} + \alpha\dot{\psi} + \beta x^2 + \beta\psi^2 + 2\beta x\psi - \gamma x^3 - 3\gamma\psi x^2 - 3\gamma x\psi^2 - \gamma\psi^3 = \sigma\cos\bar{\omega}\tau + \alpha\dot{q}_e + \left(1 + \frac{1}{3}(x + \psi) - \frac{\beta}{3}(x^2 + 2x\psi + \psi^2) + \gamma(x^3 + 3x^2\psi + 3x\psi^2 + \psi^3)\right)q_e \tag{5}$$

Averaging Eq. (5) leads to

$$\ddot{x} + x + \alpha\dot{x} + \beta x^2 + \beta\langle\psi^2\rangle - \gamma x^3 - 3\gamma x\langle\psi^2\rangle - \gamma\langle\psi^3\rangle = \sigma\cos\bar{\omega}\tau + \left\langle\left(\frac{\psi}{3} - \frac{2\beta x\psi}{3} - \frac{\beta\psi^2}{3} + 3\gamma x\psi^2 + 3\gamma x^2\psi + \gamma\psi^3\right)q_e\right\rangle \tag{6}$$

Subtracting Eq. (6) from Eq. (5) yields the equation of the fast dynamic

$$\ddot{\psi} + \psi + \alpha\dot{\psi} + \beta\psi^2 - \beta\langle\psi^2\rangle + 2\beta x\psi - 3\gamma x^2\psi - 3\gamma x\psi^2 + 3\gamma x\langle\psi^2\rangle - \gamma\psi^3 + \gamma\langle\psi^3\rangle = \alpha\dot{q}_e + \left(1 + \frac{x}{3} + \frac{\psi}{3} - \frac{\beta x^2}{3} - \frac{2\beta x\psi}{3} - \frac{\beta\psi^2}{3} + \gamma x^3 + 3\gamma x^2\psi + 3\gamma x\psi^2 + \gamma\psi^3\right)q_e - \left\langle\left(\frac{\psi}{3} - \frac{2\beta x\psi}{3} - \frac{\beta\psi^2}{3} + 3\gamma x\psi^2 + 3\gamma x^2\psi + \gamma\psi^3\right)q_e\right\rangle \tag{7}$$

This equation may be solved in rough approximation using the so-called inertial approximation, i.e., all terms in Eq. (7) containing ψ or its derivative, except the first one, are ignored [24]. Thus, the fast dynamic ψ is written as

$$\psi = \frac{\bar{a}\alpha}{\bar{\Omega}}\sin\bar{\Omega}\tau - \frac{\bar{a}}{\bar{\Omega}^2}\left(1 + \frac{x}{3} - \frac{\beta x^2}{3} + \gamma x^3\right)\cos\bar{\Omega}\tau \tag{8}$$

Inserting Eq. (8) into Eq. (6), we find the approximate equation for the slow motion

$$\ddot{x} + \omega_0^2 x + \alpha\dot{x} + \beta_1 x^2 - \gamma_1 x^3 + G_1 = \sigma\cos\bar{\omega}\tau \tag{9}$$

where ω_0^2, β_1, γ_1, and G_1 are given in the Appendix.

To examine the influence of the base displacement on the amplitude-frequency response near the two-subharmonic resonance, we express the resonance condition as

$$\omega_0^2 = \left(\frac{\bar{\omega}}{2}\right)^2 + \lambda \tag{10}$$

where λ denotes a detuning. Introducing a small bookkeeping parameter μ and scaling parameters as $\alpha = \mu\alpha$, $\beta_1 = \mu\beta_1$, $\lambda = \mu\lambda$, and $\gamma_1 = \mu^2\gamma_1$, Eq. (9) reads

$$\ddot{x} + \left(\frac{\bar{\omega}}{2}\right)^2 x = \sigma\cos\bar{\omega}\tau - G_1 + \mu(-\alpha\dot{x} - \beta_1 x^2 - \lambda x) + \mu^2\gamma_1 x^3 \tag{11}$$

Using the multiple scales method [26], we seek a solution to Eq. (11) in the form

$$x(t) = x_0(T_0, T_1, T_2) + \mu x_1(T_0, T_1, T_2) + \mu^2 x_2(T_0, T_1, T_2) + 0(\mu^3) \tag{12}$$

where $T_0 = \tau$, $T_1 = \mu\tau$, and $T_2 = \mu^2\tau$. In terms of the variables T_i, the time derivatives become $d/dt = D_0 + \mu D_1 + \mu^2 D_2 + O(\mu^3)$ and $d^2/dt^2 = D_0^2 + 2\mu D_{01} + \mu^2 D_1^2 + 2\mu^2 D_{02} + O(\mu^3)$, where $D_i = \partial/\partial T_i$. Substituting Eq. (12) into Eq. (11) and equating terms of same power of μ, we obtain the following hierarchy of problems:

$$D_0^2 x_0 + \left(\frac{\bar{\omega}}{2}\right)^2 x_0 = \sigma\cos\bar{\omega}\tau - G_1 \tag{13}$$

$$D_0^2 x_1 + \left(\frac{\bar{\omega}}{2}\right)^2 x_1 = -(2D_{01} + \alpha D_0 + \lambda)x_0 - \beta_1 x_0^2 \tag{14}$$

$$D_0^2 x_2 + \left(\frac{\bar{\omega}}{2}\right)^2 x_2 = -(2D_{01} + \alpha D_0 + \lambda)x_1 - (2D_{02} + D_{11} + \alpha D_1)x_0 - 2\beta_1 x_0 x_1 + \gamma_1 x_0^3 \tag{15}$$

The solution to the first order is given by

$$x_0(T_0, T_1, T_2) = r(T_1, T_2)\cos\left(\frac{\bar{\omega}}{2}\tau + \theta(T_1, T_2)\right) + F_1\cos(\bar{\omega}\tau) + E_1 \tag{16}$$

As usual, substituting Eq. (16) into higher-order approximations and removing secular terms, we obtain the slow flow modulation equation of amplitude and phase

$$\begin{cases} \dfrac{dr}{dt} = A_1 r + H_1 r \sin 2\theta - H_2 r \cos 2\theta, \\ r\dfrac{d\theta}{dt} = B_1 r - C_1 r^3 + H_2 r \sin 2\theta + H_1 r \cos 2\theta \end{cases} \tag{17}$$

where A_1, B_1, C_1, H_1, H_2, E_1, and F_1 are given in the Appendix. Eliminating the phase 2θ from Eq. (17), we obtain the following amplitude-frequency response equation:

$$C_1^2 r^4 - 2C_1 B_1 r^2 + A_1^2 + B_1^2 - H_1^2 - H_2^2 = 0 \tag{18}$$

Figure 2 shows the x-amplitude-frequency response near the two-subharmonic resonance, as given by Eq. (18), for two different values of the base displacement amplitude. Figure 2(*a*) shows the frequency response in the absence of the base displacement, $\bar{a} = 0$, while Fig. 2(*b*) depicts the effect of this amplitude on the frequency response for $\bar{a} = 7$. The solid line corresponds to the stable branch, while the dashed line corresponds to the unstable one. To validate the analytical approximation, we integrate Eq. (9) numerically using the fourth-order Runge–Kutta method. The comparison demonstrates excellent agreement between the numerical (circles) and analytical solutions. These figures show that as the amplitude of the base displacement increases, the frequency response shifts toward lower frequencies.

In the case of the two-superharmonic resonance, the corresponding resonance condition is expressed as

$$\omega_0^2 = (2\bar{\omega})^2 + \lambda \tag{19}$$

where λ is the detuning parameter. Introducing a bookkeeping parameter μ, Eq. (9) can be scaled as

$$\ddot{x} + (2\bar{\omega})^2 x = \sigma \cos \bar{\omega}\tau + \mu(-\alpha\dot{x} - \beta_1 x^2 - \lambda x - G_1) + \mu^2 \gamma_1 x^3 \tag{20}$$

Using the multiple scales method, a solution to Eq. (20) is sought in the form

$$x(t) = x_0(T_0, T_1, T_2) + \mu x_1(T_0, T_1, T_2) + \mu^2 x_2(T_0, T_1, T_2) + 0(\mu^3) \tag{21}$$

where T_i (with $i = 0, 1, 2$) are defined as before. Substituting Eq. (21) into Eq. (20) and equating terms of same power of μ, we obtain the following hierarchy of problems:

$$D_0^2 x_0 + (2\bar{\omega})^2 x_0 = \sigma \cos \bar{\omega}\tau \tag{22}$$

$$D_0^2 x_1 + (2\bar{\omega})^2 x_1 = -(2D_{01} + \alpha D_0 + \lambda)x_0 - \beta_1 x_0^2 - G_1 \tag{23}$$

$$D_0^2 x_2 + (2\bar{\omega})^2 x_2 = -(2D_{01} + \alpha D_0 + \lambda)x_1 - (2D_{02} + D_{11} + \alpha D_1)x_0 - 2\beta_1 x_0 x_1 + \gamma_1 x_0^3 \tag{24}$$

Substituting the first order given by

$$x_0(T_0, T_1, T_2) = r(T_1, T_2)\cos(2\bar{\omega}\tau + \theta(T_1, T_2)) + F_2 \cos(\bar{\omega}\tau) \tag{25}$$

into higher-order approximations and removing secular terms, we obtain the slow flow modulation equation of amplitude and phase

$$\begin{cases} \dfrac{dr}{dt} = A_2 r + H_3 \sin\theta + H_4 \cos\theta, \\ r\dfrac{d\theta}{dt} = B_2 r + C_2 r^3 + H_3 \cos\theta - H_4 \sin\theta \end{cases} \tag{26}$$

where the coefficients A_2, C_2, B_2, H_3, H_4, and F_2 are given in the Appendix. Eliminating the phase θ from Eq. (26), we obtain the following amplitude-frequency response equation

$$C_2^2 r^6 + 2C_2 B_2 r^4 + (A_2^2 + B_2^2)r^2 - (H_3^2 + H_4^2) = 0 \tag{27}$$

Figure 3 shows the frequency response, as given by Eq. (27), for different values of the base displacement amplitude. Figure 3(*a*) illustrates the frequency response of the two-superharmonic resonance in the absence of the fast base displacement, $\bar{a} = 0$, while Figs. 3(*b*) depict the effect on the frequency response for the value $\bar{a} = 4.5$. The solid line is the stable branch, the dashed line is the unstable one, while the circles are obtained by numerical simulations using the fourth-order Runge–Kutta method. We see that, as in the previous case, the frequency response shifts toward lower frequencies as the amplitude of the base displacement increases.

3 Case With a Fast Parametric Stiffness

Here we analyze the effect of a fast harmonic parametric stiffness on the frequency response for the forced single-sided

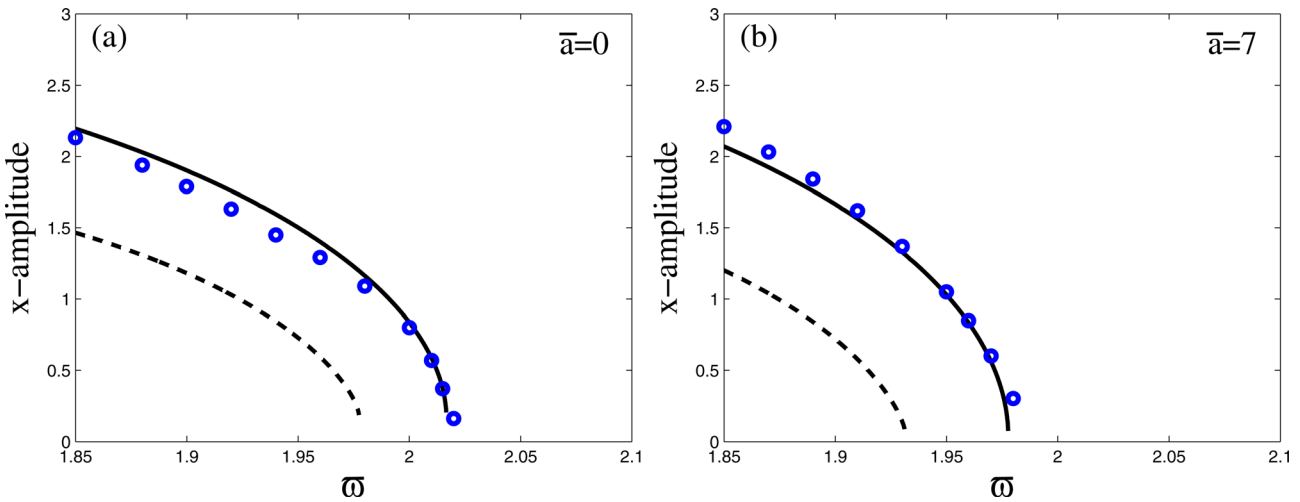

Fig. 2 Amplitude-frequency response near the two-subharmonic resonance. Analytical approximation (solid lines for stable and dashed line for unstable) and numerical simulation (circles) for $\xi = 0.01$, $\sigma = 0.5$, and $\bar{\Omega} = 8$.

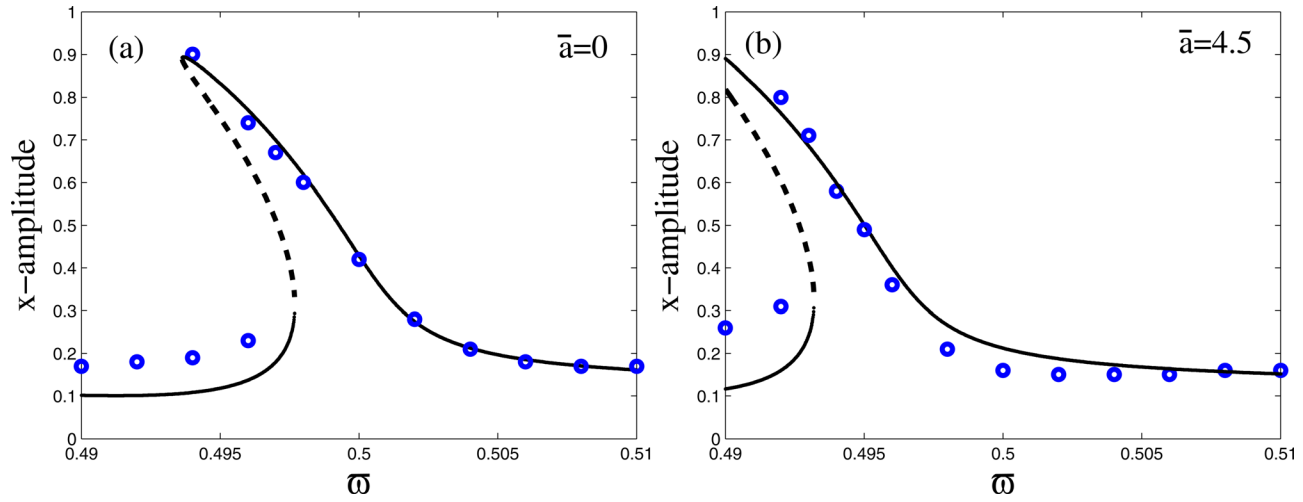

Fig. 3 Amplitude-frequency response near the two-superharmonic resonance. Analytical approximation (solid lines for stable and dashed line for unstable) and numerical simulation (circles) for $\xi = 0.001$, $\sigma = 0.1$, and $\bar{\Omega} = 8$.

Hertzian contact system considered above. In this case the schematic model is shown in Fig. 4 and the equation of motion is written as

$$m\ddot{z} + c\dot{z} + (k_0 + k_1 \cos \Omega t) z^{3/2} = N(1 + \sigma \cos(\omega t)) \tag{28}$$

Introducing the variable change $\bar{\omega} = (\omega/\nu)$, $\nu^2 = (3k_0/2m) z_s^{1/2}$, $\xi = c/2m\nu$, $\tau = \nu t$, $\bar{\Omega} = (\Omega/\nu)$, and $\bar{a} = (k_1/k_0)$, and defining $q = 3(z - z_s)/2z_s$, the dimensionless equation of motion reads

$$\ddot{q} + 2\xi\dot{q} + \left(1 + \frac{2}{3}q\right)^{3/2} + \bar{a}\left(1 + \frac{2}{3}q\right)^{3/2} \cos \bar{\Omega}\tau = 1 + \sigma \cos \bar{\omega}\tau \tag{29}$$

To analyze small vibrations around the static load, we expand in Taylor series the term $(1 + \frac{2}{3}q)^{3/2}$ up to the third order in q to obtain the equation of motion

$$\ddot{q} + q + \alpha\dot{q} + \beta q^2 - \gamma q^3 + \bar{a}(1 + q + \beta q^2 - \gamma q^3) \cos \bar{\Omega}\tau = \sigma \cos \bar{\omega}\tau \tag{30}$$

where $\alpha = 2\xi$, $\beta = \frac{1}{6}$, and $\gamma = \frac{1}{54}$. Following a similar procedure as before, we split up the motion into fast and rapid parts as

$$q(\tau) = x(T_1) + \psi(T_0, T_1) \tag{31}$$

Substituting into Eq. (30), averaging and keeping only the slow part, $x(T_1)$, the equation for the slow motion reads [9]

$$\ddot{x} + \omega_1^2 x + \alpha\dot{x} + \beta_2 x^2 - \gamma_2 x^3 + G_2 = \sigma \cos \bar{\omega}\tau \tag{32}$$

where ω_1, β_2, γ_2, and G_2 are given in the Appendix.

The two-subharmonic resonance condition is expressed as

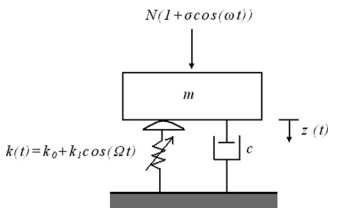

Fig. 4 Schematic model in the case of a parametric stiffness

$$\omega_0^2 = \left(\frac{\bar{\omega}}{2}\right)^2 + \lambda \tag{33}$$

with λ denotes a detuning parameter. Introducing a small parameter μ and scaling as $\alpha = \mu\alpha$, $\beta_2 = \mu\beta_2$, $\lambda = \mu\lambda$, and $\gamma_2 = \mu^2\gamma_2$, Eq. (32) reads

$$\ddot{x} + \left(\frac{\bar{\omega}}{2}\right)^2 x = \sigma \cos \bar{\omega}\tau - G_2 + \mu(-\alpha\dot{x} - \beta_2 x^2 - \lambda x) + \mu^2\gamma_2 x^3 \tag{34}$$

Using the multiple scales technique as before, the solution to the first order is given by

$$x_0(T_0, T_1, T_2) = r(T_1, T_2) \cos\left(\frac{\bar{\omega}}{2}\tau + \theta(T_1, T_2)\right) + F_3 \cos(\bar{\omega}\tau) + E_2 \tag{35}$$

where E_2 and F_3 are given in the Appendix, and the corresponding slow flow modulation equation of amplitude and phase is given by

$$\begin{cases} \dfrac{dr}{dt} = A_3 r + H_5 r \sin 2\theta - H_6 r \cos 2\theta, \\ r\dfrac{d\theta}{dt} = B_3 r - C_3 r^3 + H_6 r \sin 2\theta + H_5 r \cos 2\theta \end{cases} \tag{36}$$

where A_3, B_3, C_3, H_5, and H_6 are given in the Appendix. Eliminating the phase 2θ from the system (36), we obtain the amplitude-frequency response equation

$$C_3^2 r^4 - 2C_3 B_3 r^2 + A_3^2 + B_3^2 - H_5^2 - H_6^2 = 0 \tag{37}$$

Figures 5(*a*) and 5(*b*) depict the frequency response, as given by Eq. (37), in the absence of the amplitude of the parametric excitation, $\bar{a} = 0$ and for $\bar{a} = 3$, respectively. The stable branches (solid lines) are compared to numerical simulations using the fourth-order Runge–Kutta method (circles). In contrast to the previous case of a base displacement, here the the frequency response shifts right as the amplitude of the parametric excitation increases (see Fig. 2).

In the case of the two-superharmonic, the corresponding resonance condition is written as

$$\omega_0^2 = (2\bar{\omega})^2 + \lambda \tag{38}$$

where λ is the detuning parameter. Scaling Eq. (34) as

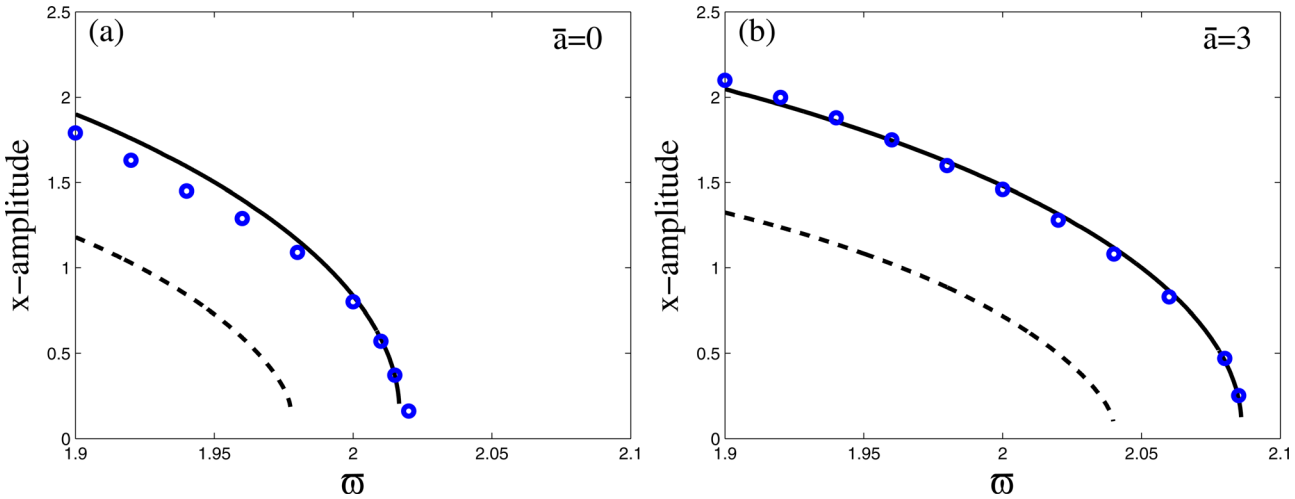

Fig. 5 Amplitude-frequency response near the two-subharmonic resonance. Analytical approximation (solid lines for stable and dashed line for unstable) and numerical simulation (circles) for $\xi = 0.01$, $\sigma = 0.5$, and $\bar{\Omega} = 8$.

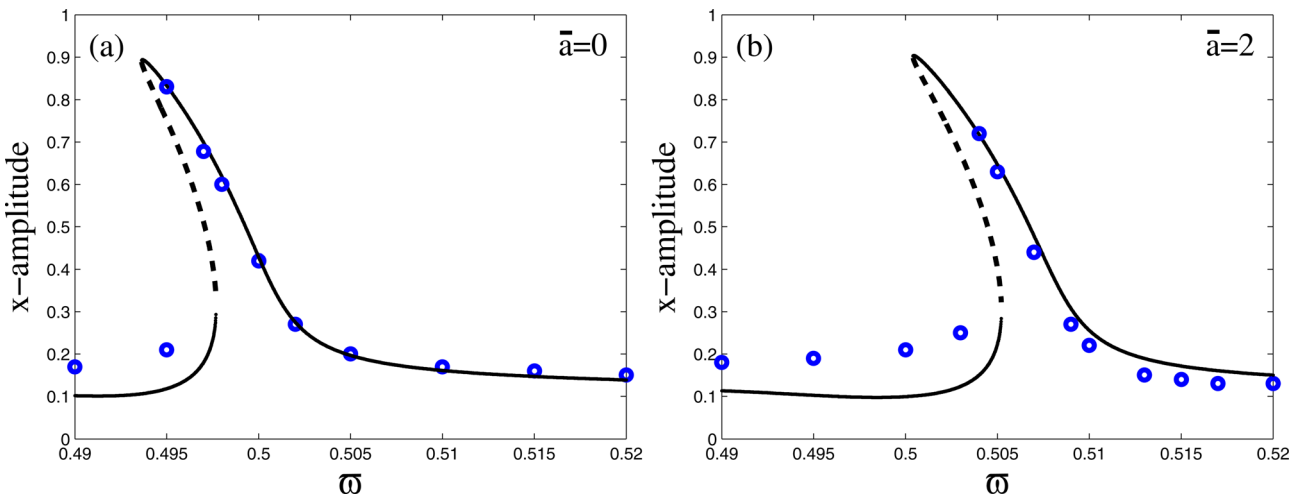

Fig. 6 Amplitude-frequency response near the two-superharmonic resonance. Analytical approximation (solid lines for stable and dashed line for unstable) and numerical simulation (circles) for $\xi = 0.001$, $\sigma = 0.1$, and $\bar{\Omega} = 8$.

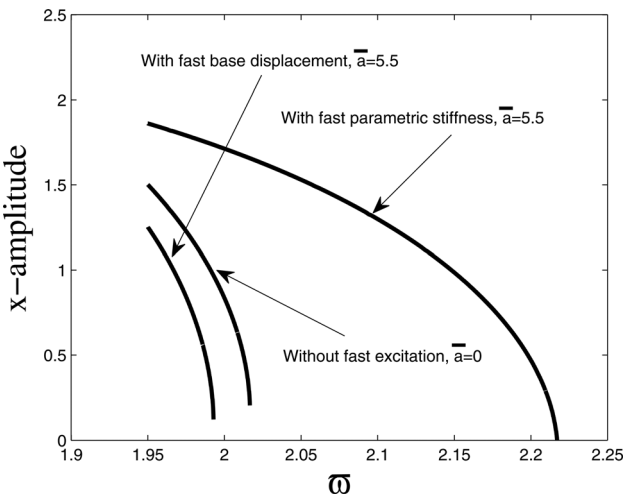

Fig. 7 Comparison of the frequency response near the two-subharmonic resonance for $\xi = 0.01$, $\sigma = 0.5$, $\bar{\Omega} = 8$ and for different values of $\bar{a}$

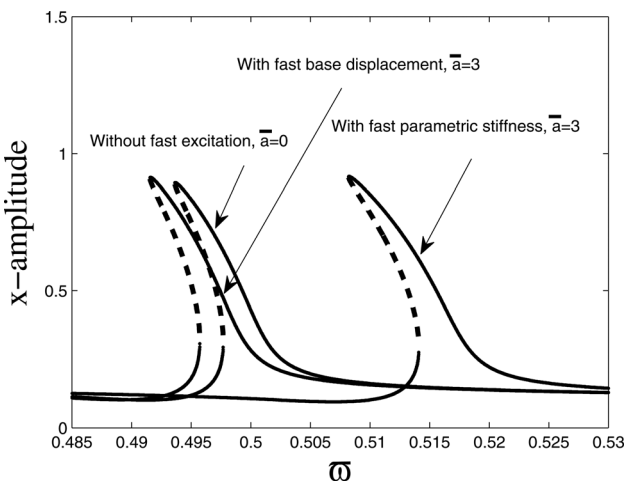

Fig. 8 Comparison of the frequency response near the two-superharmonic resonance for $\xi = 0.001$, $\sigma = 0.1$, $\bar{\Omega} = 8$ and for different values of $\bar{a}$

$$\ddot{x} + (2\bar{\omega})^2 x = \sigma\cos\bar{\omega}\tau + \mu(-\alpha\dot{x} - \beta_2 x^2 - \lambda x - G_2) + \mu^2\gamma_2 x^3 \tag{39}$$

where μ is a small parameter, and using the multiple scales method as before, we obtain the slow flow modulation equation of amplitude and phase

$$\begin{cases} \dfrac{dr}{dt} = A_4 r + H_7\sin\theta + H_8\cos\theta, \\ r\dfrac{d\theta}{dt} = B_4 r + C_4 r^3 + H_7\cos\theta - H_8\sin\theta \end{cases} \tag{40}$$

with A_4, B_4, C_4, H_7, and H_8 are given in Appendix. The corresponding amplitude-frequency response equation reads

$$C_4^2 r^6 + 2C_4 B_4 r^4 + (A_4^2 + B_4^2) r^2 - (H_7^2 + H_8^2) = 0 \tag{41}$$

Figure 6 shows the frequency response, as given by Eq. (41), near the two-superharmonic resonance for $\bar{a} = 0$ and for $\bar{a} = 2$. Here, the frequency response shifts left as $\bar{a}$ increases, whereas it shifts right when a base displacement is introduced (see Fig. 3).

4 Base Displacement Versus Parametric Stiffness

In this section, the effect of the fast base displacement and of the fast parametric stiffness on the frequency response is compared in the two cases of the sub- and superharmonic resonances of order 2. In order to appreciate how these excitations can affect the frequency response near each resonance, the comparison is carried out for the same values of the excitation amplitude $\bar{a}$.

Figure 7 compares the effect of the two excitations for the two-subharmonic resonance. It can be clearly seen that the fast parametric stiffness produces a larger shift to the right comparing to the shift caused by the fast base displacement. For presentation reasons only the stable branches of the frequency response are illustrated in the figure. Figure 8 shows the same comparison for the two-superharmonic resonance. This figure indicates that the fast parametric stiffness produces also a significant shift to the right comparing to the small shift to the left induced by the fast base displacement.

5 Conclusion

We have studied analytically the effect of a fast harmonic base displacement and of a fast harmonic parametric stiffness on vibroimpact dynamics of a forced single-sided Hertzian contact oscillator near sub- and superharmonic resonances of order 2. The technique of direct partition of motion along with the method of multiple scales were implemented to analyze the effect of the fast excitations on the occurrence of the vibroimpact regime triggered by the jump phenomenon near the resonances. We have shown that for these resonances, a fast harmonic base displacement shifts the jumps left, whereas a fast parametric stiffness shifts the jumps right.

From a practical point of view, the results indicate that, as in the case of the principal resonance [9], the control strategies can be achieved for both sub- and superharmonic resonances of order 2. Indeed, the necessary amplitude level of the fast harmonic base displacement or of the fast parametric stiffness to realize a shift remains relatively low. However, it is demonstrated that for a same value of the excitation amplitude, the fast parametric stiffness produces a larger shift of the frequency response than that produced by a fast base displacement.

Appendix

$$\omega_0^2 = \left(1 + \frac{\beta\bar{a}^2}{3\bar{\Omega}^4} - \frac{3\gamma\bar{a}^2}{2\bar{\Omega}^2}\left(\alpha^2 - \frac{1}{\bar{\Omega}^2}\right) + \frac{\gamma\bar{a}^4}{8\bar{\Omega}^4}\left(\alpha^2 + \frac{3}{\bar{\Omega}^2}\right)\right)$$

$$\omega_1^2 = 1 + \left(\beta - \frac{3}{2}\gamma\right)\frac{\bar{a}^2}{\bar{\Omega}^4} + \left(\frac{1}{2} + \beta\right)\frac{\bar{a}^2}{\bar{\Omega}^2} - \left(\frac{9\gamma\bar{a}^4}{8\bar{\Omega}^6}\right)$$

$$\beta_1 = \left(\beta - \frac{\gamma\bar{a}^2}{\bar{\Omega}^4} + \frac{\bar{a}^2}{2\bar{\Omega}^2}\left(3\gamma - \frac{\beta}{3}\right) - \frac{\gamma\bar{a}^4}{8\bar{\Omega}^4}\left(\alpha^2\beta - \frac{1}{\bar{\Omega}^2}\right)\right)$$

$$\beta_2 = \beta + \left(\beta\left(\frac{1}{2} + \beta\right) - 3\gamma\right)\frac{\bar{a}^2}{\bar{\Omega}^4} + \left(\frac{\beta}{2} + \beta - \frac{3\gamma}{2}\right)\frac{\bar{a}^2}{\bar{\Omega}^2} - \frac{9}{8}\gamma(1+\beta)\frac{\bar{a}^4}{\bar{\Omega}^6}$$

$$\gamma_1 = \left(\gamma - \frac{\beta\bar{a}^2}{\bar{\Omega}^4}\left(\gamma - \frac{\beta}{9}\right) - \frac{\bar{a}^2}{3\bar{\Omega}^2}\left(2\gamma + \frac{\beta^2}{3}\right) - \frac{\gamma\bar{a}^4}{8\bar{\Omega}^4}\left(3\gamma\alpha^2 + \frac{1}{9\bar{\Omega}^2}\right)\right)$$

$$\gamma_2 = \gamma - \left(\beta(\beta - \gamma) - \frac{3}{2}\gamma(1 + 2\beta)\right)\frac{\bar{a}^2}{\bar{\Omega}^4} + \left(\frac{\gamma}{2} - \beta^2 + \frac{3\gamma}{2}\right)\frac{\bar{a}^2}{\bar{\Omega}^2} + \frac{3}{8}\gamma(6\beta - 3\gamma + 1)\frac{\bar{a}^4}{\bar{\Omega}^6}$$

$$G_1 = \left(\alpha^2 + \frac{1}{\bar{\Omega}^2}\right)\left(\frac{\beta\bar{a}^2}{2\bar{\Omega}^2} + \frac{3\gamma\bar{a}^4}{8\bar{\Omega}^4}\right) + \frac{\bar{a}^2}{6\bar{\Omega}^2}$$

$$G_2 = \frac{\beta\bar{a}^2}{2\bar{\Omega}^4} + \frac{\bar{a}^2}{2\bar{\Omega}^2} - \frac{3\gamma\bar{a}^4}{8\bar{\Omega}^6}$$

$$A_1 = -\frac{\alpha}{2}$$

$$A_2 = -\frac{\alpha}{2} + \frac{\alpha\sigma}{16\bar{\omega}^2}$$

$$A_3 = -\frac{\alpha}{2}$$

$$A_4 = -\frac{\alpha}{2} + \frac{\alpha\sigma}{16\bar{\omega}^2}$$

$$F_1 = \frac{2\sigma}{\bar{\omega} - 2\bar{\omega}^2}$$

$$F_2 = \frac{\sigma}{3\bar{\omega}^2}$$

$$F_3 = \frac{2\sigma}{\bar{\omega} - 2\bar{\omega}^2}$$

$$E_1 = -\frac{2G_1}{\bar{\omega}}$$

$$E_2 = -\frac{2G_2}{\bar{\omega}}$$

$$H_1 = \frac{F_1\beta_1}{\bar{\omega}} + \frac{4F_1\beta_1\sigma - 9\gamma_1 F_1\bar{\omega}^2 E_1 + \gamma_1\beta_1^2 F_1 E_1}{3\bar{\omega}^3}$$

$$H_2 = \frac{4\alpha\beta_1 F_1}{3\bar{\omega}^2}$$

$$H_3 = \frac{\beta_1 F_2^2}{8\bar{\omega}} - \frac{\beta_1 F_2^2\sigma}{128\bar{\omega}^3}$$

$$H_4 = \frac{\beta_1 F_2^2\alpha}{64\bar{\omega}^2}$$

$$H_5 = \frac{F_3\beta_2}{\bar{\omega}} + \frac{4F_3\beta_2\sigma - 9\gamma_2 F_3\bar{\omega}^2 E_2 + \gamma_2\beta_2^2 F_3 E_2}{3\bar{\omega}^3}$$

$$H_6 = \frac{4\alpha\beta_2 F_3}{3\bar{\omega}^2}$$

$$H_7 = \frac{\beta_2 F_4^2}{8\bar{\omega}} - \frac{\beta_2 F_4^2 \sigma}{128\bar{\omega}^3}$$

$$H_8 = \frac{\beta_2 F_4^2 \alpha}{64\bar{\omega}^2}$$

$$B_1 = \frac{2\beta_1 E_1 + \sigma}{\bar{\omega}} - \frac{30\beta_1^2 F_1^2 + 144\beta_1^2 E_1^2 + 3\alpha^2\bar{\omega}^2 + 12\sigma^2 + 18\gamma_1 F_1^2\bar{\omega}^2 + 144\beta_1\sigma E_1 + 36\gamma_1 E_1^2\bar{\omega}^2}{12\bar{\omega}^3}$$

$$B_2 = -\left(\frac{120\bar{\omega}^2\alpha^2 + 240\beta_1 G_1 + 184\beta_1^2 F_2^2 + 720\gamma_1 F_2^2\bar{\omega}^2 + 30\sigma^2}{1920\bar{\omega}^3} - \frac{\sigma}{4\bar{\omega}}\right)$$

$$B_3 = \frac{2\beta_2 E_2 + \sigma}{\bar{\omega}} - \frac{30\beta_2^2 F_3^2 + 144\beta_2^2 E_2^2 + 3\alpha^2\bar{\omega}^2 + 12\sigma^2 + 18\gamma_2 F_3^2\bar{\omega}^2 + 144\beta_2\sigma E_2 + 36\gamma_2 E_2^2\bar{\omega}^2}{12\bar{\omega}^3}$$

$$B_4 = -\left(\frac{120\bar{\omega}^2\alpha^2 + 240\beta_2 G_2 + 184\beta_2^2 F_4^2 + 720\gamma_2 F_4^2\bar{\omega}^2 + 30\sigma^2}{1920\bar{\omega}^3} - \frac{\sigma}{4\bar{\omega}}\right)$$

$$C_1 = \frac{40\beta_1^2 + 9\gamma_1\bar{\omega}^2}{12\bar{\omega}^3}$$

$$C_2 = -\frac{360\gamma_1\bar{\omega}^2 + 100\beta_1^2}{1920\bar{\omega}^3}$$

$$C_3 = \frac{40\beta_2^2 + 9\gamma_2\bar{\omega}^2}{12\bar{\omega}^3}$$

$$C_4 = -\frac{360\gamma_2\bar{\omega}^2 + 100\beta_2^2}{1920\bar{\omega}^3}$$

References

[1] Nayak R., 1972, "Contact Vibrations," J. Sound Vib., **22**, pp. 297–322.
[2] Hess, D., and Soom A., 1991, "Normal Vibrations and Friction Under Harmonic Loads: Part 1-Hertzian Contact," ASME J. Tribol., **113**, pp. 80–86.
[3] Sabot, J., Krempf, P., and Janolin C., 1998, "Nonlinear Vibrations of a Sphere-Plane Contact Excited by a Normal Load," J. Sound Vib., **214**, pp. 359–375.
[4] Carson, R., and Johnson K., 1971, "Surface Corrugations Spontaneously Generated in a Rolling Contact Disc Machine," Wear, **17**, pp. 59–72.
[5] Soom, A., and Chen, J. W., 1986, "Simulation of Random Surface Roughness-Induced Contact Vibrations at Hertzian Contacts During Steady Sliding," ASME J. Tribol., **108**, pp. 123–127.
[6] Rigaud, E., and Perret-Liaudet, P., 2003, "Experiments and Numerical Results on Nonlinear Vibrations of an Impacting Hertzian Contact. Part 1: Harmonic Excitation," J. Sound Vib., 265, pp. 289–307.
[7] Perret-Liaudet, J., and Rigaud E., 2006, "Response of an Impacting Hertzian Contact to an Order-2 Subharmonic Excitation: Theory and Experiments," J. Sound Vib., 296, pp. 319–333.
[8] Perret-Liaudet, J., and Rigaud E., 2007, "Superharmonic Resonance of Order 2 for an Impacting Hertzian Contact Oscillator: Theory and Experiments," J. Comput. Nonlinear Dyn. 2, pp. 190–196.
[9] Bichri, A., Belhaq, M., and Perret-Liaudet J., 2011, "Control of Vibroimpact Dynamic of a Singlesided-Hertzian Contact Forced Oscillator," Nonlinear Dyn., 63, pp. 51–60.
[10] Stephenson, A., 1908, "On Induced Stability," Philos. Mag., 15, pp. 233–236.
[11] Hirsch, P., 1930, "Das pendel mit oszillierendem Aufhängepunkt," Z. Angew. Math. Mech., **10**, pp. 41–52.
[12] Kapitza, P. L., 1951, "Dynamic Stability of a Pendulum With an Oscillating Point of Suspension," Zh. Eksp. Teor. Fiz., **21**, pp. 588–597.
[13] Thomsen, J. J., 2002, "Some General Effects of Strong High-Frequency Excitation Stiffening, Biasing, and Smoothening," J. Sound Vib., **253**, pp. 807–831.
[14] Jensen, J. S., Tcherniak, D. M., and Thomsen J. J., "Stiffening Effects of High-Frequency Excitation: Experiments for an Axially Loaded Beam," J. Appl. Mech., **253**, pp. 397–402.
[15] Hansen, M. H., 2000, "Effect of High-Frequency Excitation on Natural Frequencies of Spinning Discs," J. Sound Vib., **234**, pp. 577–589.
[16] Tcherniak, D., and Thomsen, J. J., 1988, "Slow Effect of Fast Harmonic Excitation for Elastic Structures," Nonlinear Dyn., **17**, pp. 227–246.
[17] Sah, S. M., and Belhaq, M., 2008, "Effect of Vertical High-Frequency Parametric Excitation on Self-Excited Motion in a Delayed van der Pol Oscillator," Chaos Solitons Fractals, **37**, pp. 1489–1496.
[18] Belhaq, M., and Sah, S. M., 2008, "Fast Parametrically Excited van der Pol Oscillator With Time Delay State Feedback," Int. J. Non-linear Mech., **43**, pp. 124–130.
[19] Belhaq, M., and Sah, S. M., 2008, "Horizontal Fast Excitation in Delayed van der Pol Oscillator," Commun. Nonlinear Sci. Numer. Simul., **13**, pp. 1706–1713.
[20] Belhaq, M., and Fahsi, A., 2008, "2:1 and 1:1 Frequency-Locking in Fast Excited van der Pol–Mathieu–Duffing oscillator," Nonlinear Dyn., **53**, pp. 139–152.
[21] Fahsi, A., Belhaq, M., and Lakrad F., 2009, "Suppression of Hysteresis in a Forced van der Pol–Duffing Oscillator," Commun. Nonlinear Sci. Numer. Simul., **14**, pp. 1609–1616.
[22] Lakrad, F., and Belhaq M., 2011, "Suppression of Pull-in in a Microstructure Actuated by Mechanical Shocks and Electrostatic Forces," Int. J. Non-Linear Mech., **146**, pp. 407–414.
[23] Johnson, K. L., 1979, *ContactMechanics*, Cambridge University Press, Cambridge.
[24] Blekhman, I. I., 2000, *Vibrational Mechanics Nonlinear Dynamic Effects, General Approach, Application*, World Scientific, Singapore.
[25] Thomsen, J. J, 2003, *Vibrations and Stability: Advanced Theory, Analysis, and Tools*, Springer-Verlag, Berlin.
[26] Nayfeh, A. H., and Mook, D. T., 1979, *Nonlinear Oscillations*, Wiley, New York.